PHYSICAL REVIEW C VOLUME 26, NUMBER 4 OCTOBER 1982

Changes of charge radii and hyperfine interactions of the Dy isotopes

D. L. Clark
Nuclear Structure Research Laboratory, University of Rochester, Rochester, New York 14627

G. W. Greenlees
Department of Physics, University of Minnesota, Minneapolis, Minnesota 55455

(Received 16 February 1982)

A continuous wave dye laser and a thermal atomic beam were used to measure the optical isotope shifts and hyperfine splittings for the 5547 Å, 5639 Å, 5652 Å, 5974 Å, and the 5989 Å transition of the seven stable isotopes of dysprosium. The hyperfine splitting of the odd-A isotopes has been analyzed using the formalism of Sanders and Beck and the hyperfine anomaly has been extracted. Comparison with calculations using Nilsson wave functions is presented. The isotope shift measurements have been analyzed with published electronic and muonic x-ray isotope shifts to yield $\delta\langle r^2\rangle$ values and some estimates of the specific mass shift constant.

[NUCLEAR STRUCTURE $^{156-164}$Dy. Measured optical isotope shifts and hyperfine splittings. Deduced $\delta\langle r^2\rangle$, $A(4f^{12}6s\,6p)$, $B(4f^{12}6s\,6p)$, and the hyperfine anomaly. Laser spectroscopy on atomic beams.]

I. INTRODUCTION

The development of dye lasers has revitalized the study of optical spectra as a source of nuclear properties. The high resolution of the laser systems enables precision measurements of isotope shifts and hyperfine interactions and the high sensitivity of optical techniques allows measurements on extremely small quantities of material. There are data presently available for laser studies on nuclei far from stability[1] and more experimental efforts using a variety of techniques are presently underway.[1–3] The results reported here are part of a series of measurements on the isotope shifts and hyperfine structure of the naturally occurring even-Z rare-earth elements. Most of the even-Z rare-earth elements have seven stable isotopes and the hyperfine spectra of the odd-A isotopes are complex. High resolution laser spectroscopy of thermal atomic beams makes possible detailed measurements of these complex spectra using natural abundance samples.

This paper reports measurements of the hyperfine splitting and isotope shifts of five optical transitions for the naturally occurring dysprosium isotopes. Information has been obtained on the changes of the nuclear mean square radii and the hyperfine interactions of the two odd-A isotopes have been analyzed to obtain information on the differences in spatial distribution of nuclear magnetism.

This is the second report of measurements in the rare-earth region. The earlier paper, Ref. 4, reported results for ytterbium and contains a detailed discussion of the formalism for the analysis of the data. The procedures for the analysis of the dysprosium data are very similar to that of the ytterbium data, so much of the present discussion will be abbreviated and reference made to the more complete discussion in Ref. 4. Equations taken from Ref. 4 will be indicated by the corresponding equation numbers preceded by a Roman I. The analysis of the hyperfine anomaly of the odd-A dysprosium isotopes has been the subject of a previous short publication.[5]

II. EXPERIMENTAL METHOD

The experimental technique has also been described in detail in Ref. 4. Briefly, a tunable dye laser is incident on a collimated thermal atomic beam at right angles. Scattered photons are collected by a lens system and focused onto a photomultiplier (PMT). The PMT pulse rate is converted to an analog signal which is the vertical signal on an X-Y plotter. The horizontal signal is the sweep voltage of the dye laser. Frequency interval markers are provided by a Fabry-Perot interferometer which is electro-optically locked to a Lamb-dip sta-

TABLE I. Isotopic abundance and nuclear spin of dysprosium isotopes.

A	I	%
156	0	0.052
158	0	0.090
160	0	2.29
161	$\frac{5}{2}$	18.88
162	0	25.53
163	$\frac{5}{2}$	24.97
164	0	28.18

bilized He-Ne laser. The frequency intervals between resonance peaks are determined by interpolation.

III. EXPERIMENTAL DATA AND ANALYSIS

Measurements were made of the isotope shifts and hyperfine splittings of the seven isotopes of Dy for five optical transitions using natural abundance samples. Table I lists the natural abundance of the Dy isotopes. The basic atomic characteristics of the ground and excited states[6] of the transitions studied are given in Table II. All the transitions are from the lowest member of the ground state multiplet, which is a $4f^{10}6s^2$ configuration and is predominantly a $^5I_8$ term type. The excited states of the transitions studies are nearly pure configurations. Four are predominantly $4f^{10}6s\,6p$ and one is $4f^9 5d\,6s^2$. This means four of the transitions should show a negative isotope shift and one should show a positive isotope shift as was observed.

A spectrum obtained for the 5974.5 Å transition, which has a negative isotope shift, is shown in Fig. 1. Owing to the high J values for the ground and excited states and the nuclear spin of $\frac{5}{2}$ for both odd isotopes, the hyperfine splitting is rather complex.

Wide sweeps, such as the one shown in Fig. 1, do not accurately show the laser system's ability to resolve the hyperfine splitting; this is shown in the narrow sweep of Fig. 2. This figure also shows the close frequency interval markers which are, in this case, 36.02 MHz apart. These close markers are generated by shifting the Fabry-Perot locking mode

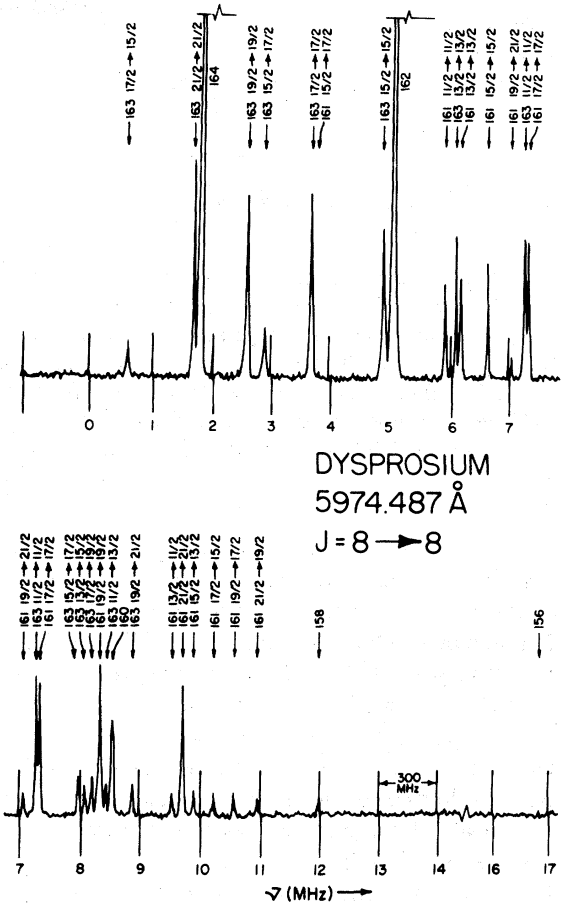

FIG. 1. Spectra for the 5974.5 Å transition of neutral dysprosium. The peaks are labeled according to isotope and F quantum number for the odd A isotopes. The numbered markers are generated by a frequency stabilized Fabry-Perot etalon and are 300.36 MHz apart.

TABLE II. Atomic level characteristics of transitions measured. The configurations and term types are for the largest component of the wave function. Detailed wave functions and configurations are contained in Table V.

λ (Å)	J_g	J_{ex}	Ground state	Excited state
5547.268	8	8	$4f^{10}6s^2(^5I_8)$	$4f^{10}6s\,6p(^5K_8)$
5639.498	8	9	$4f^{10}6s^2(^5I_8)$	$4f^{10}6s\,6p(^5K_9)$
5652.009	8	7	$4f^{10}6s^2(^5I_8)$	$4f^9 5d\,6s^2(^7K_7)$
5974.487	8	8	$4f^{10}6s^2(^5I_8)$	$4f^{10}6s\,6p(^5I_8)$
5988.562	8	7	$4f^{10}6s^2(^5I_8)$	$4f^{10}6s\,6p(^5H_7)$

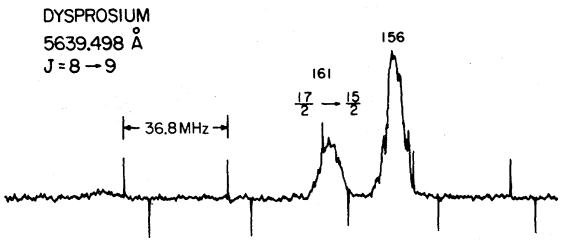

FIG. 2. Narrow sweep of some weak lines in the 5639.5 Å transition of neutral dysprosium. The peaks are labeled according to isotope and F quantum number for the ^{161}Dy line. The close frequency markers shown are 36.02 MHz apart and are generated by a frequency stabilized Fabry-Perot etalon. The ^{156}Dy is a rare isotope which is 0.052% abundant in the natural abundance sample.

as described in Ref. 4. It has been possible to identify every line seen in the hyperfine splitting and to locate in the spectrum every allowed transition. The line due to the very rare isotope ^{156}Dy (0.052%) and a very weak hyperfine line are clearly visible which demonstrates that measurements on such rare isotopes can be performed with essentially the same accuracy, limited only by systematic errors, as can be achieved for more abundant isotopes.

Occasionally, there are lines which are within just a few MHz of each other which cannot be resolved. This prevented measurements of the line due to ^{158}Dy for the 5652 Å transition even though the blended lines were identified in the spectrum. Usually closely spaced hyperfine lines are not a problem, since only one of the transitions from the ground state hyperfine multiplet to each of the excited state levels is needed to determine the excited state splitting. The 5547 Å transition had several very close lines which made it necessary to use some blended lines in the hyperfine splitting analysis of that transition. The results of all the measurements are tabulated in the Appendix. Table III lists the measured isotope shifts for the five transitions along with the small amount of published x ray[7] and muonic atom[8] data. The present measurements are generally in good agreement with the previously published results[9–12] except for a few comparisons with the data of Ref. 12 which disagree by a few standard deviations.

A. Analysis of the hyperfine splitting

The magnetic dipole and electric quadrupole coupling constants for the excited states of the transitions are deduced as described in the Appendix and are given in Table IV. The experimental errors in the quantities are based on ±0.5 MHz accuracy in the line positions.[4] The magnetic octupole coupling constants were less than experimental errors in all cases.

The analysis of the Yb hyperfine splitting contained in Ref. 4 describes the methods used to determine the contributions of s and p electrons to the hyperfine splitting and the hyperfine anomaly (HFA). The analysis of the Dy case proceeds along similar lines, but is more complex due to the unfilled $4f$ shell which results in many more components in the intermediate coupled wave function. The basic equations required have been developed in Sec. IV A of Ref. 4.

The wave functions of Griffith, Ross, and Cowan[13] were used with additional information on some of the smaller components of the wave functions as provided by Cowan.[14] The coefficients of

TABLE III. Experimental data on the isotope shifts in DyI. The available x ray and muonic atoms isotope shifts data are also listed.

		Optical isotope shifts (MHz)					x ray i.s. (Ref. 7)	Muonic i.s. (Ref. 8)
A_1	A_2	5547.268	5639.498	5652.009	5974.487	5988.562	(meV)	(keV)
162	164	−1008.0	−1006.0	1120.2	−975.6	−866.0	55.6(3.7)	10.066(500)
160	162	−1089.8	−1089.8	1235.1	−1053.3	−932.4		
158	160	−1077.1	−1073.8		−1046.6	−923.0		
156	158	−1597.3	−1594.5		−1532.2	−1357.6		
156	160		−2668.3	3204.3		−2280.6		
162	163	−321.4	−319.5	272.8	−311.7	−281.7	4.2(3.3)	
160	161	−283.9	−285.1	210.2	−277.2	−250.4		
161	162		−804.7	1024.9			39.4(5.1)	
163	164		−686.5				51.4(4.7)	
161	163	−1127.3	−1124.2	1297.8	−1087.9	−963.6		

TABLE IV. The magnetic hyperfine coupling constant, A, and the electric quadrupole coupling constant, B, for ^{161}Dy and ^{163}Dy for the excited state in the transitions measured. All values are in MHz. The excited state configurations and J values are according to Wyart (Ref. 6).

λ (Å)	Config.	J	A(161)	A(163)	B(161)	B(163)
5988.562	$4f^{10}6s\,6p$	7	−64.286(17)	89.858(17)	892.2(9)	943.2(9)
5974.487	$4f^{10}6s\,6p$	8	−88.657(14)	123.998(14)	1401.3(9)	1481.2(9)
5652.009	$4f^{9}5d\,6s^2$	7	−112.874(16)	158.054(16)	2432.3(9)	2575.1(9)
5639.492	$4f^{10}6s\,6p$	9	−148.004(13)	207.295(13)	1561.0(9)	1652.2(9)
5547.268	$4f^{10}6s\,6p$	8	−110.191(14)	154.326(14)	589.9(9)	618.3(9)

the components are tabulated in Table V. Using these wave functions and standard angular momentum coupling techniques it is possible to write the matrix elements for the dipole and quadrupole coupling constants A and B

$$A=\left[\frac{1}{IJ}\right]A_1=(\mu_I/IJ)\langle\gamma JJ\mid T_E^{(1)}\mid\gamma JJ\rangle\ ,$$
$$B=4A_2=2eQ\langle\gamma JJ\mid T_E^{(2)}\mid\gamma JJ\rangle\ , \tag{I8}$$

in terms of sums of reduced matrix elements of $T_E^{(1)}$,

$$\begin{aligned}T_E^{(1)}=&\mu_0\sum_i\frac{4}{3}\left\langle\frac{\delta(r_i)}{r_i^2}\right\rangle_{10}s_i+2\left\langle\frac{1}{r_i^3}\right\rangle_{01}l_i\\&+2\sqrt{10}\left\langle\frac{1}{r_i^3}\right\rangle_{12}(s_iC^{(2)})^{(1)}\ ,\\T_E^{(2)}=&e\sum_i\left\langle\frac{1}{r_i^3}\right\rangle_{11}(s_il_i)^{(2)}\\&+\left\langle\frac{1}{r_i^3}\right\rangle_{13}[s_i(C_i^{(4)}l_i)^{(3)}]^{(2)}\\&-\left\langle\frac{1}{r_i^3}\right\rangle_{02}C_i^{(2)}\ ,\end{aligned} \tag{I15}$$

TABLE V. Wave functions of the excited states with a $4f^{10}6s\,6p$ configuration (Refs. 13 and 14). The basis wave functions are of the type $|4f^{10}(S_1L_1J_1K_1)6s\,6p\,(S_2L_2J_2)J\rangle$. The classification of states is that of Nielson and Koster (Ref. 30). The index K labels states with the same SLJ but different parentage.

		$C_J(S_1L_1J_1K_1S_2L_2J_2)$			
		5988.6	5974.5	5547.3	5639.5
$(S_1L_1J_1K_1)$	$(S_2L_2J_2)$	$J=7$	$J=8$	$J=8$	$J=9$
$^5I_80$	$^3P_0$	0	0.44287	0.08256	0
	$^3P_1$	−0.93588	0.83020	0.18868	0.25059
	$^3P_2$	0.11069	−0.19866	0.94230	0.93863
	$^1P_1$	−0.16947	0.14131	−0.00485	0.04241
$^5I_70$	$^3P_0$	0.16166	0	0	0
	$^3P_1$	−0.08775	0.09546	−0.08966	0
	$^3P_2$	−0.2289	0.00493	0.13292	0.09644
	$^1P_1$	−0.00144	0.01147	−0.01459	0
$^3K_81$	$^3P_0$	0	0.04732	0.00694	0
	$^3P_1$	−0.09777	0.08358	0.02367	0.02798
	$^3P_2$	0.01355	−0.01937	0.09260	0.09307
	$^1P_1$	−0.01944	0.01459	0.00124	0.00437
$^3K_82$	$^3P_0$	0	−0.09039	−0.01196	0
	$^3P_1$	0.18845	−0.16048	−0.04700	−0.05263
	$^3P_2$	−0.02792	0.03548	−0.17767	−0.18051
	$^1P_1$	0.03830	−0.02682	−0.00081	−0.00842
$^3K_72$	$^3P_0$	−0.02193	0	0	0
	$^3P_1$	0.01285	−0.01263	0.01068	0
	$^3P_2$	0.00080	−0.00123	−0.01621	−0.01254
	$^1P_1$	0.00092	−0.00139	0.00175	0

for the configurations $4f^{10}$ and $6s\,6p$.[15,16] The angular momentum factors in these matrix elements can be evaluated by well known but, for complex wave functions such as these, lengthy computations. The calculations were accomplished by means of a computer program that accepts as input the necessary coefficients of fractional parentage and yields as output the coefficients of the seven relativistic radial integrals. For example, for the 5988.6 Å excited state of ^{163}Dy the expression is

$$\begin{aligned} A =& 0.627\left\langle\frac{\delta(r)}{r^2}\right\rangle_{10}(s)-0.051\left\langle\frac{\delta(r)}{r^2}\right\rangle_{10}(p) \\ &-2.065\left\langle\frac{1}{r^3}\right\rangle_{10}(p)-1.729\left\langle\frac{1}{r^3}\right\rangle_{12}(p) \\ &+4.576\left\langle\frac{\delta(r)}{r^2}\right\rangle_{10}(f)+21.909\left\langle\frac{1}{r^3}\right\rangle_{01}(f) \\ &-2.594\left\langle\frac{1}{r^3}\right\rangle_{12}(f) . \end{aligned} \tag{3}$$

There are seven unknown radial integrals but measurements of A and wave functions are available for only four transitions. In order to reduce the number of unknowns to fewer than the number of equations we use the relativistic correction factors (RCF) as described in Eq. (16) of Ref. 4. In this way the number of unknown radial integrals is reduced to three. For example, Eq. (3) becomes

$$\begin{aligned} A =& -0.627\left\langle\frac{\delta(r)}{r^2}\right\rangle_{10}(s)-5.696\left\langle\frac{1}{r^3}\right\rangle_{\mathrm{NR}}(p) \\ &+21.768\left\langle\frac{1}{r^3}\right\rangle_{\mathrm{NR}}(f) , \end{aligned} \tag{4}$$

where radial integrals are given in units of $a_0{}^{-3}$ and A is in MHz. The coefficients of the radial integrals for the four excited states are given in Table VI. We now have four equations with three unknowns which we can solve for the radial integrals by minimizing the squared error of the fit to the dipole coupling constants. This yields the radial integrals:

$$\begin{aligned} &a_0{}^3\left\langle\frac{\delta(r)}{r^2}\right\rangle_{10}(s)=123.9 , \\ &a_0{}^3\left\langle\frac{1}{r^2}\right\rangle_{\mathrm{NR}}(p)=3.69 , \\ &a_0{}^3\left\langle\frac{1}{r^3}\right\rangle_{\mathrm{NR}}(f)=8.62 . \end{aligned} \tag{5}$$

The f electron radial integral can be compared to the ground state value measured by Childs.[7] Using the RCF value for the ratio of the relativistic and nonrelativistic radial integral [Eq. (I16)] we obtain

$$a_0{}^3\left\langle\frac{1}{r^3}\right\rangle_{01}(f)=8.68 ,$$

which is in very good agreement with the value 8.72(4) obtained by Childs. The fitted values of the dipole coupling constants (Table VII) show a maximum deviation from the experimental values of 2.5%. These two comparisons indicate the procedure used is satisfactory within the limits required.

The finite size of the distribution of nuclear magnetism has a small but measurable effect on the magnetic dipole coupling constant, A. This is observed in the optical measurements as a variation in the ratio of the magnetic dipole coupling constants of the odd-A isotopes for different electronic transitions. This ratio varies because the transitions have different contributions to the hyperfine splitting from the $s_{1/2}$ and $p_{1/2}$ electrons which have significant density within the nucleus and consequently are sensitive to the finite extent of the nuclear magnetism. The effects of the finite nuclear size on the magnetic dipole coupling constant are parametrized by the equation

$$\frac{A(1)}{A(2)}=\frac{g_I(1)(1-\epsilon(1))}{g_I(2)(1-\epsilon(2))}=\frac{g_I(1)}{g_I(2)}(1-\Delta_{12}) , \tag{I9}$$

TABLE VI. Coefficients of the radial integrals for the s, p, and f electrons in the equation for the magnetic dipole coupling constant, A. See Eqs. (3) and (4).

	s		p			f			
λ (Å)	$\left\langle\frac{\delta(r)}{r^2}\right\rangle_{10}$	$\left\langle\frac{\delta(r)}{r^2}\right\rangle_{10}$	$\left\langle\frac{1}{r^3}\right\rangle_{01}$	$\left\langle\frac{1}{r^3}\right\rangle_{12}$	$\left\langle\frac{1}{r^3}\right\rangle_{\mathrm{NR}}$	$\left\langle\frac{\delta(r)}{r^2}\right\rangle_{10}$	$\left\langle\frac{1}{r^3}\right\rangle_{01}$	$\left\langle\frac{1}{r^3}\right\rangle_{12}$	$\left\langle\frac{1}{r^3}\right\rangle_{\mathrm{NR}}$
5988.6	−0.627	−0.051	−2.065	−1.729	−5.696	4.576	21.909	−2.594	21.768
5974.5	−0.483	−0.279	1.481	1.613	4.807	4.068	19.250	−0.207	19.150
5639.5	0.421	0.293	2.335	−0.470	2.123	3.552	16.952	−0.177	16.862
5547.3	−0.058	−0.042	1.255	0.290	1.116	3.854	18.801	−0.187	18.711

TABLE VII. The ratios of hyperfine coupling constants, the hyperfine anomaly (HFA) parameter Δ, and the contributions of $s_{1/2}$ and $p_{1/2}$ electrons to Δ. The fifth column gives the ratio of the experimental magnetic dipole coupling constant to the value computed using radial integrals determined using the procedure described in the text. The contributions of $s_{1/2}$ and $p_{1/2}$ electrons to Δ are computed using the same radial integrals.

λ (Å)	$A(163)/A(161)$	Δ(%)	$\Delta(s_{1/2},p_{1/2})$	$\frac{A(\text{expt})}{A(\text{calc.})}$	$\frac{B(163)}{B(161)}$
5988.6	−139779(44)	−0.176(36)	$-0.8727\Delta(s_{1/2})-0.1352\Delta(p_{1/2})$	0.991	1.0572(11)
5974.5	−1.39863(27)	−0.116(19)	$-0.4867\Delta(s_{1/2})+0.0898\Delta(p_{1/2})$	0.991	1.0570(10)
5652.0	−1.40027(25)	0.001(17)			1.0587(6)
5639.5	−1.40061(15)	0.025(11)	$0.2544\Delta(s_{1/2})+0.0036\Delta(p_{1/2})$	0.991	1.0584(8)
5547.3	−1.40052(23)	0.019(16)	$-0.0447\Delta(s_{1/2})+0.0032\Delta(p_{1/2})$	1.025	1.0541(23)

where Δ_{12} is the hyperfine anomaly (HFA) parameter and the ratio of the g factors is determined by a technique which is not sensitive to the finite nuclear size. This is normally taken from nuclear magnetic resonance (NMR) measurements but in the case of Dy no such measurements are available. Since the hyperfine splitting of the 5652.01 Å transition is due to f and d electrons, which do not have significant density at the nucleus, the HFA should be zero. Consequently we take the ratio of the A's for this transition to be equal to the ratio of the g factors to compute the HFA parameters listed in Table VIII. No second-order corrections have been made but they are expected to be small.

Using the radial integrals obtained from the analysis of the hyperfine splittings, expressions for the HFA parameter can be written in terms of the HFA parameters of the $s_{1/2}$ and $p_{1/2}$ electrons. These expressions are also given in Table VII. Figure 3 shows the experimental results displayed as a function of mutually consistent values of $\Delta(s_{1/2})$ and $\Delta(p_{1/2})$. The widths of the bands reflect experimental errors only and do not include additional errors to compensate for inaccuracies in the atomic wave functions or in the procedure used to reduce the number of radial integrals involved. Reasonable agreement is seen between the results for the three usable cases.

A calculation of $\Delta(s_{1/2})$ as a function of deformation has been performed using Nilsson wave functions[18] in a manner similar to the Yb calculations. The results are summarized in Table VIII where it can be seen that the computed values of Δ and g_k agree with the experimental value for $\beta \approx 0.2$ to 0.3. The small computed values of Δ are differences of the ϵ values which are much larger and assume the deformation parameter β is the same for ^{161}Dy and ^{163}Dy. The g_k results show that

$$(g_s)_{\text{eff}} \cong 0.7(g_s)_{\text{free}}$$

(Ref. 20). The same sort of renormalization should be required for the spin contributions to ϵ. Since neither the renormalization effect or the deformation are exactly the same for the ^{161}Dy and ^{163}Dy isotopes the level of agreement between the calculated and experimental values is satisfactory for $\beta \cong 0.3$ which is the accepted value.[21]

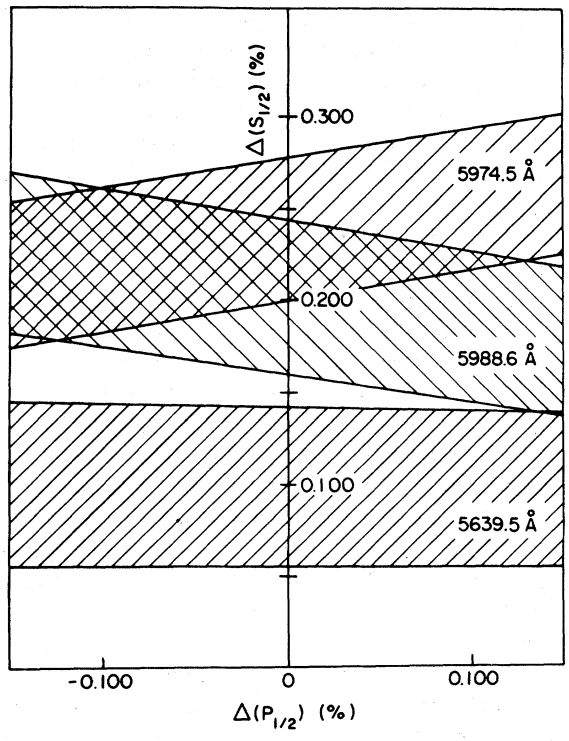

FIG. 3. Hyperfine anomalies, Δ, for $s_{1/2}$ and $p_{1/2}$ electrons in Dy. The bands indicate mutually consistent combinations of $\Delta(s_{1/2})$ and $\Delta(p_{1/2})$ compatible with the experimental measurements for the three transitions. The width of the band indicates the experimental error in the dipole coupling constant.

TABLE VIII. Magnetic moment and hyperfine anomaly parameters computed using Nilsson wave functions (Ref. 18) for the $\frac{5}{2}^+[642]$ orbital for ^{161}Dy and the $\frac{5}{2}^-[523]$ orbital for ^{163}Dy. The μ_I values of Ref. 19 were used in the calculation of ϵ. For the calculation of g_k, the neutron spin gyromagnetic ratio g_s was renormalized by 0.7 (Ref. 20). The experimental values for g_k were taken from Ref. 20.

	^{161}Dy		^{163}Dy		
β	g_k	ϵ (%)	g_k	ϵ (%)	Δ (%)
0.3	−0.33	3.11	0.32	3.41	0.30
0.2	−0.29	2.75	0.23	2.90	0.15
0.1	−0.24	2.37	0.04	1.51	−0.86
0.0	−0.21	2.05	0.24	2.67	0.62
−0.1	−0.18	1.83	0.23	2.84	1.01
−0.2	−0.17	1.74	0.24	2.64	0.90
−0.3	−0.19	1.99	0.22	2.93	0.96
Expt.	−0.34		+0.25		0.15

B. Analysis of isotope shifts

The isotope shift data listed in Table III has been used to construct the King plot shown in Fig. 4. The available x-ray isotope shift data is also plotted. On the scale of Fig. 4 the optical isotope shift (i.s.) data form very good straight lines. Figure 5 shows on an expanded scale the deviations from a straight line fit to the even isotope pairs. The even-even isotope pairs show small but significant deviations from the straight line. The odd-odd isotope pair lies very close to the straight line fit but the odd-even pairs are several standard deviations away, particularly in the case of the 5974.5 transition. Similar deviations have been observed in erbium and samarium.[22] These deviations may be due to second-order effects in the monopole term of the hyperfine interaction.[4] Griffith *et al.*[23] have reported deviations for even-even isotopes as large as 30 MHz in some transitions in Sm. They have suggested that they are due to mixing of nearby levels induced by second-order terms involving combinations of mass shift and hyperfine interaction operators. The cause of these shifts remains to be established.

The slopes of the lines relative to the 5639.5 Å line are listed in Table IX and are seen to be closely correlated with the configuration of the excited state as determined by Wyart.[6] Assigning a slope of 1.0 to the $f^{10}sp$ configurations, −1.69 to the f^9ds^2, and neglecting the small contribution of the f^9d^2s yields 1.00, 1.00, 0.973, 0.839, and −1.56 for the slopes as listed in Table IX. Such correlations between slopes and configurations have been used to help assign configurations to unknown spectra.[24]

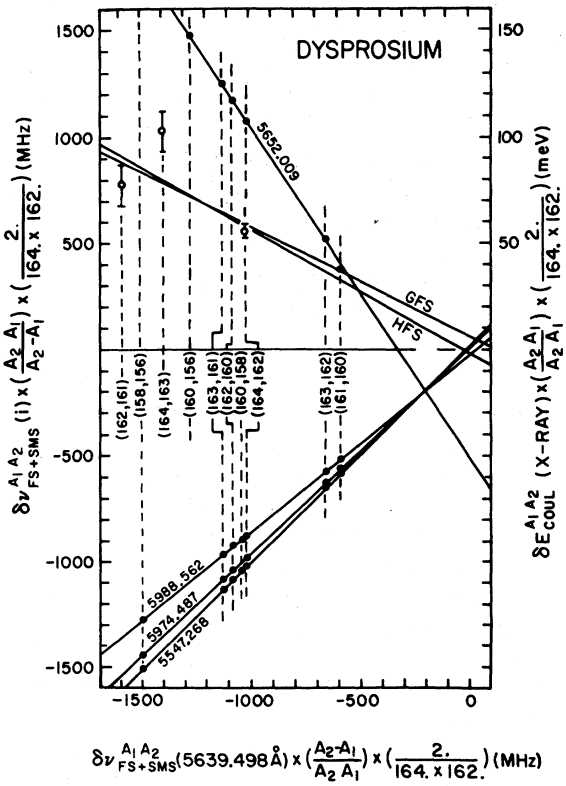

FIG. 4. King plot of the optical isotope shifts for five transitions on neutral dysprosium. The available x-ray isotope data (Ref. 8) are also plotted. The GFS and HFS lines correspond to simultaneous fits to the x-ray data and a muonic atoms isotope shift data point using $R=1.445$ and F_i computed using the Goudsmit-Fermi-Segre method (GFS) or derived from the analysis of the hyperfine splitting, as described in the text.

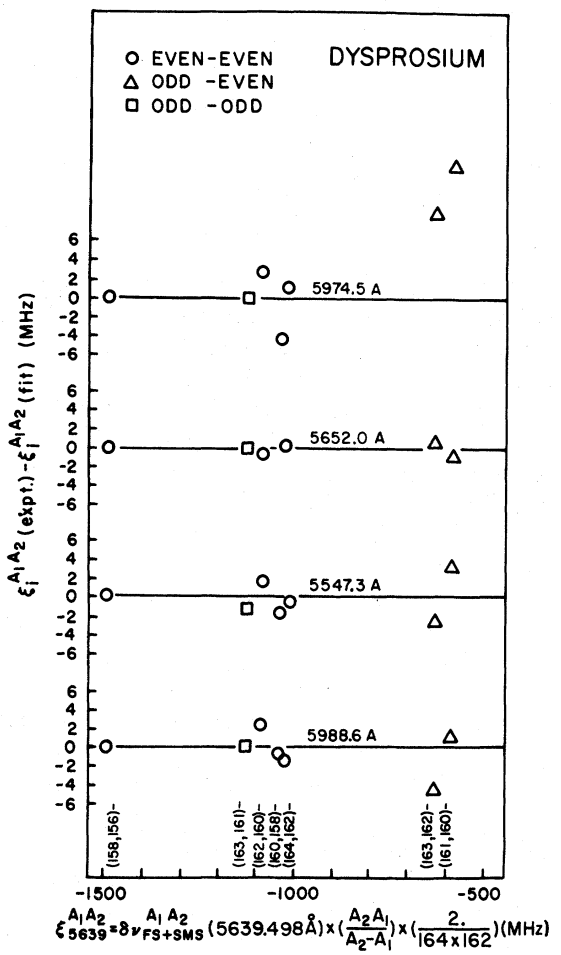

FIG. 5. Deviations of the optical isotope shift data from a straight line fit on a King plot. The deviations are too small to be visible on Fig. 4 but as shown here are significantly larger than the experimental errors which are approximately the size of the data points.

The level of precision of this method is unknown. For example, in the present case, the slope of the 5974.5 Å line would imply a somewhat stronger admixture of f^9ds^2. It is also possible that other configurations need to be admixed.

The isotope shifts can be written as a sum of two parts, the field shift and the mass shift:

$$\delta\nu_i^{A_1A_2}=F_i\lambda^{A_1A_2}+\left[\frac{A_2-A_1}{A_1A_2}\right]\times(M_{i,\text{normal}}+M_{i,\text{specific}})\,, \qquad \text{(I22,I29)}$$

where F_i is the isotope shift constant and M_i designates either the normal mass shift (NMS) constant or the specific mass shift (SMS) constant. The NMS constant is easily determined using

TABLE IX. Slopes of lines on the Dy King plot.

λ (Å)	Slope	Configuration (Ref. 6) $f^{10}sp$	f^9ds^2	f^9d^2s
5639.5	1	100	0	0
5547.3	1.0015(18)	100	0	0
5974.5	0.9391(18)	99	1	0
5988.6	0.8341(17)	94	6	0
5652.0	−1.5616(51)	4	95	1

$$M_{i,\text{normal}}=\nu_i/1836.1$$

(Ref. 18). (It is conventional to use the proton mass, $m_p/m_e=1836$ instead of the atomic mass unit when computing the NMS. The motivation for this convention is not clear but the difference is only 0.7% so that the distinction is unimportant.) The points plotted in Fig. 4 have been corrected for the NMS. The nuclear parameter $\lambda^{A_1A_2}$ is defined by

$$\lambda^{A_1A_2}=\delta\langle r^2\rangle^{A_1A_2}+(C_2/C_1)\delta\langle r^4\rangle^{A_1A_2}+\cdots\,. \qquad \text{(I28)}$$

In order to determine $\lambda^{A_1A_2}$ from the measured values of $\delta\nu_i^{A_1A_2}$, F_i, and $M_{i,\text{specific}}$ must be determined for one of the transitions. Since the 5639.5 and the 5547.3 Å transitions involve nearly pure configurations, these were chosen. F_i for the other transitions can be obtained from the slopes listed in Table IX.

Two methods can be employed to compute the isotope shift constant, F_i. The analysis of the hyperfine splitting yields a value of the radial integral for the contact interaction. Following the procedure described in Ref. 4, and using the value of

$$\left\langle\frac{\delta(r)}{r^2}\right\rangle_{10}(s)$$

from Eq. (5) and a screening ratio $\gamma'=0.88$ (Refs. 26 and 27) yields

$$F_i=-7.20\ \text{GHz/fm}^2\,.$$

Also the Goudsmit-Fermi-Segre (GFS) value of F_i can be computed. Using the value of $E_i=0.417$ determined by Sugar and Reader[28] and the shielding factor $\gamma=0.72$ (Refs. 26 and 27) yields

$$F_i = -8.14 \text{ GHz/fm}^2 .$$

The GFS value of F_i is 13% higher than the HFS value. This is a somewhat worse agreement than the 5% difference found in the case of Yb.

The SMS constant can be determined from a fit to a King plot of the x-ray isotope shifts and muonic atom isotope shift data versus the optical isotope shift data. Data from the 5639.5 Å line are used. In order to include the muonic atom isotope shift data point in the fit it must be corrected for the fact that the muonic isotope shifts are sensitive to

$$\delta\langle r^k e^{-\alpha r}\rangle^{A_1 A_2}$$

instead of $\lambda^{A_1 A_2}$. The procedure for requiring the King plot fits to have the same horizontal intercept (i.e., the same SMS) and requiring the ratio of the x-ray and muonic slopes to be compatible with theory is described in detail in Ref. 4. Briefly, the ratio of the slopes is given by

$$\frac{(\text{slope})_{\text{x ray}}}{(\text{slope})_{\text{muonic}}} = \left[\frac{C_1}{BZ}\right] \frac{\lambda}{\delta\langle r^k e^{-\alpha r}\rangle} , \qquad \text{(I34)}$$

where the parameter R is defined by

$$R \equiv \frac{\lambda}{\delta\langle r^k e^{-\alpha r}\rangle} .$$

The tables of Engfer *et al.*[8] can be used to find $BZ = 102.6$ keV/fm^k. Seltzer[29] has computed $C_1 = 423$. The value of R can be estimated by considering a nuclear charge distribution given by

$$\rho(r) = \rho_0 \left\{1 + \exp\left[\frac{4\ln 3(r-c)}{t}\right]\right\}^{-1}$$

Numerical integration yields

$$\lambda = 44.61\left[\frac{\delta c}{c}\right] + 6.98\left[\frac{\delta t}{t}\right] ,$$

and

$$\delta\langle r^k e^{-\alpha r}\rangle = 30.87\left[\frac{\delta c}{c}\right] + 4.28\left[\frac{\delta c}{t}\right] ,$$

using $c = 6.284$ fm, $t = 2.3$ fm, $k = 2.326$, $\alpha = 0.137$ fm^{-1}, and $c_2/c_1 = -8.62\times10^{-4}$ fm^{-2}.[7,8] These results yield

$$R = 1.445\left[\frac{1 + 0.427\left[\frac{\delta t}{\delta c}\right]}{1 + 0.379\left[\frac{\delta c}{\delta c}\right]}\right] .$$

If $\delta t = 0$, $R = 1.445$. If $\delta t = \delta c$, $R = 1.495$. If all the change in λ is due to skin thickness change, $R = 1.629$.

Simultaneous fits of the muonic atom data point and the x-ray data were made using F_i and R as variable parameters. The χ^2 contour plot is shown in Fig. 6. The GFS and HFS values of F_i are indicated and the $t = 0$ value of R is labeled. The minimum of χ^2 is rather shallow due to the rather poor fit of the x-ray data as can be seen in Fig. 4. The GFS and HFS values for F_i and the $\delta t = 0$ value of R are near the χ^2 minimum. At the $\delta t = 0$ value of R, SMS is + 122 MHz for the GFS value of F_i and −22 MHz for the HFS value of F_i. At a fixed value of F_i, SMS increases about 50 MHz for a 10% increase in R. The previous analysis of the optical isotope shifts (Refs. 9, 12, 24, and 25) used a value of F_i about equal to the present GFS value and a SMS of zero or half the NMS (about 10 MHz). That combination of parameters does not result in a minimum squared error fit to the x ray and muonic data except for a very small value of R, but, considering the small amount of muonic and x-ray data and the poor fit of the data for any set of parameters, it is not unreasonable. The previous analysis of the Yb isotope shift data, where the x-ray and muonic atom isotope shift data were better, indicated that the specific mass shift was about 10 times the normal mass shift.

Here the GFS fit to the muonic and x-ray data is used to compute λ, and experimental errors are assigned based on a variation of ± 100 MHz in the SMS. This should be a reasonable estimate of the possible error and results in $\sim 10\%$ error in the values of λ. A comparison of the results of our analysis and that of previous analyses of optical, x ray, and muonic i.s. is presented in Table X. The isotope shifts of the 5639.5 Å line have been used. The small but consistent difference between the present results and previous optical i.s. results is almost entirely due to the difference in the SMS. The 164-162 point agrees well with the x ray and muonic atoms data, but the odd-A x-ray points do not show as good agreement. As was discussed in Ref. 4, the relative values of λ between isotope pairs is much more accurately determined than is λ. In the case of Dy, the odd isotopes are very close to the even A isotope one mass unit lighter. This uneven

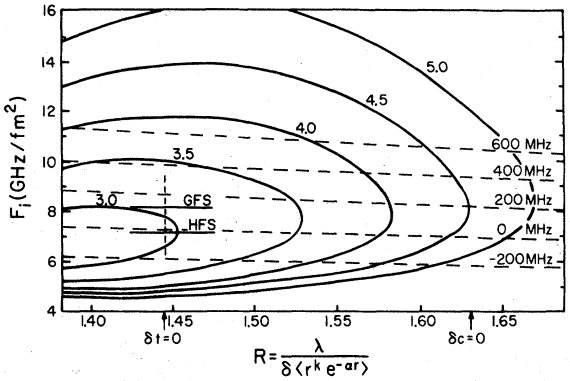

FIG. 6. Contours of χ^2 (solid lines) and specific mass shift (dashed lines) in the R,F_i plane. The available x-ray and muonic atoms isotope shift data are simultaneously fit to the optical isotope shift data for the 5639.5 Å transition. The Goudsmit-Fermi-Segre (GFS) and hyperfine splitting (HFS) values of F_i are shown. The vertical dashed line indicates the value of R for no change in the skin thickness parameter t. The GFS and HFS lines shown in Fig. 4 correspond to the intersection of the $\delta t=0$ line and the GFS and HFS lines.

spacing results in a larger error in the relative λ. For example $\lambda^{160,161}/\lambda^{156,158}$ is 0.216 and varies 22% for a change of 100 MHz in the SMS, whereas $\lambda^{158,160}/\lambda^{160,162}$ is 0.965 and varies only 0.28%.

This work was supported by the National Science Foundation under Grant No. PHY-82-40321 and Grant No. PHY-79-21336.

APPENDIX

The results of the measurements are tabulated in this appendix. All values are in MHz. $\delta\nu$ for the even isotopes are relative to the transition due to ^{164}Dy. For the odd A isotopes, the ground state is indicated by F and the excited state by F'. The measured values, $\delta\nu(F,F')$, are line positions relative to the ^{164}Dy line. These values are used with the equation

$$\sum_F (2F+1)\Delta E_F=0 \tag{I6}$$

to compute the center of gravity (COG) of the splitting. Equation (I6) does not include the effect of second order and higher terms. The $\delta\nu(F,F')$ values are used with the ground state hyperfine splitting, $\delta\nu(F)$, obtained from the measurements of Childs,[17] to compute the excited state hyperfine splitting, $\delta\nu(F')$ (see Table XI). The listed values of $\delta\nu(F)$ and $\delta\nu(F')$ are relative to zero and the COG of the excited state, respectively. The ^{158}Dy line of the 5652 Å transition was not completely resolved so no measurement was made.

The magnetic dipole and electric quadrupole coupling constants A and B were extracted using the formalism described in Ref. 4. Briefly, the first order perturbation energies are given by

$$\Delta E_F^{(1)}=(-1)^{I+J+F} \times\sum_k \left[\begin{Bmatrix} JIF \\ IJk \end{Bmatrix} \Big/ \begin{bmatrix} JkJ \\ J0J \end{bmatrix} \begin{bmatrix} IkI \\ I0I \end{bmatrix}\right] A_k \cdot \tag{I5}$$

For those transitions where the splitting of all the components of the excited states have been measured this expression can be inverted to determine A_k from the measured values of ΔE_F:

TABLE X. A comparison of experimental results for $\lambda^{A_1A_2}$ and $\delta\langle r^k e^{-ar}\rangle^{A_1A_2}$ for Dy isotopes. The previously reported results are from Refs. 7, 8, 12, and 25. $\delta\langle r^k e^{-ar}\rangle$ was computed from the reported i.s. using $C=102.6$ keV/fm^k. λ has been obtained from $\delta\langle r^k e^{-ar}\rangle$ using $R=1.44$ which is computed assuming $\delta t=0$.

				$\lambda^{A_1A_2}$			$\delta\langle r^k e^{-ar}\rangle$
A_1	A_2	This analysis	Optical i.s.	x ray i.s.	x ray + optical	Muonic i.s.	Muonic i.s.
164	162	0.141(12)	0.133(10)	0.130(9)	0.125(7)	0.141(7)	0.098(5)
162	160	0.152(12)	0.144(11)		0.134(11)		
150	158	0.150(12)	0.142(10)		0.126(11)		
158	156	0.215(12)	0.211(15)		0.242(17)		
163	161	0.156(12)	0.150(11)				
164	163	0.093(6)	0.091(10)	0.120(11)			
163	162	0.048(6)	0.042(3)	0.010(8)	0.015(4)		
162	161	0.108(6)		0.092(12)	0.114(7)		
161	160	0.044(6)	0.036(3)				

TABLE XI. Compilation of the measured line positions relative to the ^{164}Dy line and the ground and excited state hyperfine splittings. The center of gravity (COG) of the hyperfine splittings of the odd isotopes is also listed.

5547.268 Å			161		1813.9 (COG)			163		686.6 (COG)	
A	$\delta\nu$	F	F'	$\delta\nu(F,F')$	$\delta\nu(F)$	$\delta\nu(F')$	F	F'	$\delta\nu(F,F')$	$\delta\nu(F)$	$\delta\nu(F')$
164	0	$\frac{11}{2}$	$\frac{11}{2}$	1498.9	3004.07	2689.2	$\frac{11}{2}$	$\frac{11}{2}$	684.3	−3251.26	−3253.5
162	1008.0	$\frac{13}{2}$	$\frac{13}{2}$	1694.2	1911.55	1791.7	$\frac{13}{2}$	$\frac{13}{2}$	796.0	−2549.31	−2439.9
160	2097.8	$\frac{15}{2}$	$\frac{15}{2}$	1851.2	794.21	831.6	$\frac{15}{2}$	$\frac{15}{2}$	852.7	−1588.05	−1422.0
158	3175.0	$\frac{17}{2}$	$\frac{17}{2}$	1944.0	−286.54	−129.4	$\frac{17}{2}$	$\frac{17}{2}$	825.7	−302.63	−163.5
156	4772.3	$\frac{19}{2}$	$\frac{19}{2}$	1944.0	−1261.11	−1131.0	$\frac{15}{2}$	$\frac{17}{2}$	2111.1	−1588.05	−163.6
		$\frac{21}{2}$	$\frac{21}{2}$	1809.6	−2051.72	−2056.3	$\frac{19}{2}$	$\frac{19}{2}$	684.3	1380.43	1378.2
							$\frac{21}{2}$	$\frac{21}{2}$	385.3	3543.29	3242.0

5639.498 Å			161		1810.6 (COG)			163		686.5 (COG)	
A	$\delta\nu$	F	F'	$\delta\nu(F,F')$	$\delta\nu(F)$	$\delta\nu(F')$	F	F'	$\delta\nu(F,F')$	$\delta\nu(F)$	$\delta\nu(F')$
164	0	$\frac{11}{2}$	$\frac{13}{2}$	3042.2	3004.07	4235.6	$\frac{11}{2}$	$\frac{13}{2}$	−679.2	−3251.26	−4616.9
162	1006.0	$\frac{17}{2}$	$\frac{15}{2}$	4739.6	−286.54	2642.4	$\frac{13}{2}$	$\frac{15}{2}$	−335.2	−2549.31	−3571.0
160	2095.8	$\frac{13}{2}$	$\frac{15}{2}$	2542.4	1911.55	2643.3	$\frac{15}{2}$	$\frac{17}{2}$	107.3	−1588.05	−2167.2
158	3169.6	$\frac{17}{2}$	$\frac{17}{2}$	3143.9	−286.54	1046.7	$\frac{17}{2}$	$\frac{19}{2}$	668.6	−302.63	−319.9
156	4764.0	$\frac{15}{2}$	$\frac{17}{2}$	2064.9	794.21	1048.5	$\frac{19}{2}$	$\frac{21}{2}$	1365.9	1380.43	2059.9
		$\frac{19}{2}$	$\frac{19}{2}$	2596.5	−1261.11	−475.3	$\frac{21}{2}$	$\frac{23}{2}$	2220.7	3543.36	5077.5
		$\frac{17}{2}$	$\frac{19}{2}$	1622.3	−286.54	−474.9					
		$\frac{19}{2}$	$\frac{21}{2}$	1235.5	−1261.11	−1836.2					
		$\frac{21}{2}$	$\frac{23}{2}$	922.8	−2051.72	−2939.6					

5652.009 Å			161		−2145.2 (COG)			163		−847.4 (COG)	
A	$\delta\nu$	F	F'	$\delta\nu(F,F')$	$\delta\nu(F)$	$\delta\nu(F')$	F	F'	$\delta\nu(F,F')$	$\delta\nu(F)$	$\delta\nu(F')$
164	0	$\frac{11}{2}$	$\frac{9}{2}$	−1983.1	3004.07	1020.9	$\frac{11}{2}$	$\frac{9}{2}$	205.4	−3251.21	−3045.9
162	−1120.2	$\frac{11}{2}$	$\frac{11}{2}$	−3352.5	3004.07	−348.4	$\frac{11}{2}$	$\frac{11}{2}$	280.4	−3251.21	−2970.9
160	−2355.3	$\frac{13}{2}$	$\frac{11}{2}$	−2261.8	1911.55	−350.2	$\frac{13}{2}$	$\frac{11}{2}$	−421.4	−2549.31	−2970.7
156	−5559.6	$\frac{13}{2}$	$\frac{13}{2}$	−3567.6	1911.55	−1656.1	$\frac{15}{2}$	$\frac{13}{2}$	−963.3	−1588.05	−2551.3
		$\frac{15}{2}$	$\frac{15}{2}$	−3537.9	794.21	−2743.7	$\frac{17}{2}$	$\frac{15}{2}$	−1316.9	−302.63	−1619.5

TABLE XI. (*Continued.*)

5652.009 Å			161		−2145.2 (COG)			163		−847.4 (COG)	
		$\frac{17}{2}$	$\frac{17}{2}$	−3143.9	−286.54	−3430.5	$\frac{19}{2}$	$\frac{17}{2}$	−1367.6	1380.43	12.9
		$\frac{19}{2}$	$\frac{17}{2}$	−2170.7	−1261.11	−3431.8	$\frac{17}{2}$	$\frac{17}{2}$	315.1	−302.63	12.4
		$\frac{21}{2}$	$\frac{19}{2}$	−1406.2	−2051.72	−3512.0	$\frac{15}{2}$	$\frac{17}{2}$	1600.6	−1588.05	12.5
							$\frac{21}{2}$	$\frac{19}{2}$	−982.1	3543.29	2561.2
							$\frac{19}{2}$	$\frac{19}{2}$	1184.1	1380.43	2564.6
							$\frac{17}{2}$	$\frac{19}{2}$	2867.9	−302.63	2563.7

5974.487 Å			161		1751.77 (COG)			163		1192.72 (COG)	
A	$\delta\nu$	F	F'	$\delta\nu(F,F')$	$\delta\nu(F)$	$\delta\nu(F')$	F	F'	$\delta\nu(F,F')$	$\delta\nu(F)$	$\delta\nu(F')$
164	0	$\frac{11}{2}$	$\frac{11}{2}$	1241.1	3004.07	4245.8	$\frac{11}{2}$	$\frac{11}{2}$	1652.7	−3251.26	−1598.5
162	975.58	$\frac{13}{2}$	$\frac{13}{2}$	1325.1	1911.55	3236.7	$\frac{11}{2}$	$\frac{13}{2}$	2000.6	−3251.26	−1250.6
160	2028.93	$\frac{15}{2}$	$\frac{15}{2}$	1462.8	794.21	2257.0	$\frac{13}{2}$	$\frac{13}{2}$	1298.6	−2549.31	−1250.7
158	3075.53	$\frac{17}{2}$	$\frac{17}{2}$	1669.7	−286.54	1383.1	$\frac{15}{2}$	$\frac{15}{2}$	934.7	−1588.05	−653.3
156	4607.78	$\frac{19}{2}$	$\frac{19}{2}$	1969.2	−1261.11	708.1	$\frac{17}{2}$	$\frac{17}{2}$	578.7	−302.63	276.1
		$\frac{21}{2}$	$\frac{21}{2}$	2381.1	−2051.72	329.4	$\frac{17}{2}$	$\frac{19}{2}$	1930.6	−302.63	1628.6
							$\frac{19}{2}$	$\frac{19}{2}$	248.3	1380.43	1628.8
							$\frac{21}{2}$	$\frac{21}{2}$	−29.0	3543.29	3514.3

5988.562 Å			161		1547.9 (COG)			163		584.3 (COG)	
A	$\delta\nu$	F	F'	$\delta\nu(F,F')$	$\delta\nu(F)$	$\delta\nu(F')$	F	F'	$\delta\nu(F,F')$	$\delta\nu(F)$	$\delta\nu(F')$
164	0	$\frac{11}{2}$	$\frac{9}{2}$	163.2	3004.07	3167.2	$\frac{11}{2}$	$\frac{9}{2}$	2391.0	−3251.26	−860.3
162	866.0	$\frac{13}{2}$	$\frac{11}{2}$	627.4	1911.55	2539.0	$\frac{13}{2}$	$\frac{11}{2}$	1892.9	−2549.31	−656.5
160	1799.4	$\frac{15}{2}$	$\frac{13}{2}$	1116.0	794.21	1910.2	$\frac{15}{2}$	$\frac{13}{2}$	1292.9	−1588.05	−295.1
158	2721.4	$\frac{17}{2}$	$\frac{15}{2}$	1625.8	−286.54	1339.3	$\frac{17}{2}$	$\frac{15}{2}$	587.8	−302.63	285.2
156	4079.0	$\frac{19}{2}$	$\frac{17}{2}$	2154.5	−1261.11	893.3	$\frac{19}{2}$	$\frac{17}{2}$	−255.5	1380.43	1155.0
		$\frac{21}{2}$	$\frac{19}{2}$	2697.9	−2051.72	646.2	$\frac{21}{2}$	$\frac{19}{2}$	−1150.9	3543.29	2392.4

$$A_k = \begin{Bmatrix} JkJ \\ J0J \end{Bmatrix} \begin{Bmatrix} IkI \\ I0I \end{Bmatrix} (2k+1) \times \sum_F (-1)^{I+J+F} (2F+1) \begin{Bmatrix} JIF \\ IJK \end{Bmatrix} \Delta E_F^{(1)} . \quad \text{(I7)}$$

The experimental values for $\delta\nu(F')$ are substituted for $\Delta E_F^{(1)}$ and yield A_k in MHz. If not all the components of the excited state were measured, Eq. (I5) was used to perform a least squared error fit of A_1, A_2, and A_3 to the experimental data. In those cases where both methods could be used there was no significant difference in the result. Equations (I5) and (I7) are valid only for first order splitting. Small corrections are required for higher-order terms but these corrections are difficult and require knowledge of the wave functions of the perturbing levels. These corrections have not been made but are expected to be very small. The values for A_k are used with Eq. (I8) of the text to obtain A and B.

[1]E. W. Otten, *Proceedings of the Fourth International Conference on Nuclei Far From Stability, Helsingor, Denmark, 1981* (CERN, Geneva, 1981).

[2]C. N. Davids, G. W. Greenlees, M. A. Finn, D. A. Lewis, and R. M. Evans, *Proceedings of the Fourth International Conference On Nuclei Far From Stability, Helsingor, Denmark, 1981* (CERN, Geneva, 1981).

[3]D. L. Clark, A. G. Martin, N. G. Nicolis, S. Banerjee, T. M. Cormier, P. M. Stwertka, B. S. Lin, and M. G. Herman, *Proceedings of the Fourth International Conference On Nuclei Far From Stability, Helsingor, Denmark, 1981* (CERN, Geneva, 1981).

[4]D. L. Clark, M. E. Cage, D. A. Lewis, and G. W. Greenlees, Phys. Rev. A 20, 239 (1979).

[5]D. L. Clark, M. E. Cage, and G. W. Greenlees, Phys. Lett. 62A, 439 (1977).

[6]J. F. Wyart, Physica 75, 371 (1974).

[7]F. Boehm and P. L. Lee, At. Data Nucl. Data Tables 14, 605 (1974).

[8]R. Engfer, H. Schneuwley, J. L. Viulleumier, H. K. Walter, and A. Zehnder, At. Data Nucl. Data Tables 14, 509 (1974).

[9]J. W. M. Dekkar, P. F. A. Klinkenberg, and J. F. Langkemper, Physica 39, 393 (1968).

[10]P. Grundevik, M. Gustavsson, and S. Svandberg, Phys. Lett. 56A, 25 (1976).

[11]W. J. Childs and L. S. Goodman, J. Opt. Soc. Am. 67, 747 (1977).

[12]W. Hogervorst, G. J. Zaal, J. Bouma, and J. Blok, Phys. Lett. 65A, 220 (1978).

[13]D. C. Griffith, J. S. Ross, and R. D. Cowan, J. Opt. Soc. Am. 62, 571 (1972).

[14]R. D. Cowan, private communication.

[15]P. G. H. Sandars and J. Beck, Proc. R. Soc. London Ser. A289, 97 (1965).

[16]L. Armstrong, Jr., *Theory of Hyperfine Structure of Free Atoms* (Wiley-Interscience, New York, 1971).

[17]W. J. Childs, Phys. Rev. A 2, 1692 (1970).

[18]J. P. Davidson, *Collective Models of the Nucleus* (Academic, New York, 1968), Appendix D, p. 183.

[19]J. Ferch, W. Dankworth, and H. Gebauer, Phys. Lett. 49A, 287 (1974).

[20]A. Bohr and B. R. Mottelson, *Nuclear Structure* (Benjamin, New York, 1975), Vol. II, p. 302.

[21]K. E. G. Lobner, M. Vetter, and V. Honig, Nucl. Data Tables A7, 495 (1970).

[22]D. L. Clark and G. W. Greenlees (unpublished).

[23]J. A. R. Griffith, G. R. Isaak, R. New, and M. P. Ralls, J. Phys. B 14, 2769 (1981).

[24]A review of the previous literature can be found in J. Bauche and R. J. Campeau, Ad. At. Mol. Phys. 12, 39 (1976).

[25]K. Heileg and A. Steudel, At. Data Nucl. Data Tables 14, 613 (1974).

[26]M. Wilson, J. Phys. B 5, 218 (1972).

[27]M. A. Coulthard, J. Phys. B 6, 23 (1973).

[28]J. Sugar and J. Reader, J. Opt. Soc. Am. 55, 1286 (1965).

[29]E. C. Seltzer, Phys. Rev. 188, 1916 (1969).

[30]C. W. Nielson and G. F. Koster, *Spectroscopic Coefficients for p^n, d^n, and f^n Configurations* (MIT, Cambridge, Mass., 1963).